Int J Adv Manuf Technol (2017) 91:2419–2426
DOI 10.1007/s00170-016-9954-9

ORIGINAL ARTICLE

Scanning speed and powder flow rate influence on the properties of laser metal deposition of titanium alloy

Rasheedat M. Mahamood[1,2] · **Esther T. Akinlabi**[1]

Received: 30 September 2016 / Accepted: 20 December 2016 / Published online: 5 January 2017

Abstract Ti4Al4V is an important aerospace alloy because of its excellent properties that include high strength-to-weight ratio and corrosion resistance. In spite of these impressive properties, processing titanium is very challenging which contributes to the high cost of the material. Laser metal deposition, an important additive manufacturing method, is an excellent alternative manufacturing process for Ti6Al4V. The economy of this manufacturing process also depends on the right combination of processing parameters. The principal aim of this study is to know the optimum processing parameters that will result in deposit with sound metallurgical bonding with the substrate with proper mechanical property and better surface finish. This will help to reduce the need for expensive secondary finishing operations using this manufacturing process. This study investigates the influence of scanning speed and the powder flow rate on the resulting properties of the deposited samples. Microstructure, microhardness, and surface finish of Ti6Al4V samples were produced using the laser metal deposition process over a range of scanning speeds, ranging from 0.02 to 0.12 m/s, and powder flow rate, ranging from 0.72 to 6.48 g/min. The microstructure, microhardness, and surface finish were characterized using optical microscopy, Metkon hardness tester, and Jenoptik surface analyzer, respectively. These process parameter variations were mapped with the microstructure, the microhardness, and surface roughness. The microstructures were found to change from the thick lath of basket woven to martensitic microstructure as the scanning speed and the powder flow rate were increased. The microhardness and the surface roughness were found to increase as the scanning speed and the powder flow rate were increased. It can be concluded that in order to minimize the surface roughness while maintaining a moderate microhardness value, the optimum scanning speed is about 0.63 m/s while the powder flow rate should be maintained at 2.88 g/min. The laser power and the gas flow rate should also be fixed at 3 kW and 2 l/min, respectively.

Keywords Additive manufacturing · Mechanical properties · Optical microscopy · Powder flow rate · Scanning speed · Surface roughness

1 Introduction

Laser metal deposition process belongs to the directed energy deposition class of additive manufacturing that can produce three-dimensional (3D) objects directly from the 3D computer-aided design (CAD) by incrementing the material layer by layer [1]. In this process, the laser is focused on the substrate, thereby creating a melt pool on the substrate. The powder or wire material is then delivered into the melt pool causing the delivered materials to be melted and upon solidification forming a track of the deposited material that is metallurgically bounded to the substrate. Laser metal deposition process is a promising advanced manufacturing process that is capable of reducing the buy-to-fly ratio and also capable of repairing high-valued parts that were prohibitive or not repairable in the past [2–4]. Laser metal deposition process, like any additive manufacturing, is a tool-less manufacturing process making it an ideal alternative manufacturing process for difficult-to-machine materials such as titanium and its alloys.

Ti6Al4V is an important titanium alloy, and it is the most commonly produced and the most widely used titanium alloy

✉ Rasheedat M. Mahamood
mahamoodmr2009@gmail.com

[1] University of Johannesburg, Johannesburg, South Africa

[2] University of Ilorin, Ilorin, Nigeria

[5]. Ti6Al4V is often referred to as the workhorse of the industry because of the excellent properties possessed by the alloy [6]. These properties include high strength-to-weight ratio, excellent corrosion resistance, and heat treatability [7]. The use of laser metal deposition to produce or repair high-valued parts is an interesting research area because of the great potential of this manufacturing technology [3, 4, 8–17]. Processing parameters play an important role in the properties of the deposited parts [11, 13, 18–23].

The aim of this study is to establish the influence of scanning speed and the powder flow rate on the evolving physical, metallurgical, and mechanical properties of the deposited samples. The properties that are investigated are respectively the surface roughness, the microstructure, and the microhardness. This study will help to establish the optimized processing parameter that will give optimized surface finish and better mechanical property. This will help to reduce the need for secondary finishing operation after the deposition of the part. The results are presented and discussed in detail.

2 Materials and methods

In this study, an experimental set-up available at the National Laser Center, CSIR, Pretoria, South Africa as shown pictorially in Fig. 1 was used [20]. The experimental set-up consists of a Kuka robot that carries Nd-YAG laser and co-axial powder nozzles in its end effector. The Nd-YAG laser is of maximum power output of 4 kW with wavelength of 1.06 μm because of its suitability for processing this type of material [24]. The controlled environment chamber was improvised by using plastic wrapping, argon gas, and box, as shown in Fig. 1, helps to prevent contamination of the deposited samples from the atmospheric oxygen and nitrogen by keeping the oxygen level below 10 ppm. The laser focal length is maintained at a distance of 195 mm above the substrate and with a spot size of 2 mm.

The substrate materials and the powder material used in this study is Ti6Al4V of 99.6% purity. The substrate is a hot rolled sheet of 70 × 70 × 5 mm dimension. The Ti6Al4V powder is gas atomized powder. The substrate was sandblasted and washed with acetone before the deposition process. The laser power was maintained at a value of 3.0 kW and the gas flow rate at a value of 2 l/min throughout the experiments. Experimental matrix with varying scanning speeds and varying powder flow rates are shown in Tables 1 and 2, respectively.

After the deposition process, the as-deposited sample was washed with acetone before the surface roughness measurements. The surface roughness of each track of the samples was measured with stylus surface analyzer by Jenoptik, equipped with Hommelmap 6.2 software. The measuring condition was in accordance with the "BS EN ISO 4288:1998" standard

Fig. 1 Experimental set-up [20]

[25]. Five measurements were taken on each of the samples, and the arithmetic average of the 2D roughness profiles (R_a) was recorded. The samples for the microhardness and the microstructure were then cut in the vertical direction of the deposited track so as to reveal the cross-section of the samples. The cut samples were mounted in resin ground and polished following the standard metallurgical preparation of titanium and its alloys [26]. The samples for microstructural examination were etched using Kroll's reagent, and the microstructure was studied under an Olympus BX51M optical microscope (OP) equipped with an Olympus DP25 digital camera. The microhardness indentation was taken using a Vickers microhardness indenter with a load of 300 g and a dwelling time of 15 s according to the ASTM E92-16 standard [27]. The distance between indentations was maintained at 15 μm. The distance of 15 μm between indentations was chosen because

Table 1 Experimental matrix with varying scanning speeds

Sample label	Scanning speed (m/s)	Powder flow rate (g/min)
A1	0.02	2.88
A2	0.04	2.88
A3	0.06	2.88
A4	0.08	2.88
A5	0.1	2.88
A6	0.12	2.88

Table 2 Experimental matrix with varying powder flow rates

Sample label	Powder flow rate (g/min)	Scanning speed (m/s)
B1	0.72	0.06
B2	1.44	0.06
B3	2.88	0.06
B4	4.32	0.06
B5	5.76	0.06
B6	6.48	0.06

it is more than twice the size of indentation which is recommended by the ASTM standard.

3 Results

The microstructure of the Ti6Al4V substrate is shown in Fig. 2a. The morphology of the Ti6Al4V powder is shown in Fig. 2b. The micrographs of the deposited samples A1, A6, B1, and B5 are shown in Fig. 3a, b, c, and d, respectively. The micrographs showing the microstructure of samples produced at a scanning speed of 0.06 m/s and powder flow rate of 0.72 g/min is shown in Fig. 4a and that of the sample at a scanning speed of 0.06 m/s and powder flow rate of 6.48 g/min is shown in Fig. 4b. The results of the effect of the varying scanning speed on the microhardness and the average surface roughness are presented in Table 3. The results of the influence of the powder flow rate on the microhardness and average surface roughness are presented in Table 4. The microhardness indentation produced on the sample deposited at a scanning speed of 0.04 and powder flow rate of 2.88 g/min is shown in Fig. 5. The graph of the microhardness and surface roughness against the scanning speed is shown in Fig. 6a, and the graph of microhardness and surface roughness versus powder flow rate is shown in Fig. 6b.

4 Discussion

The microstructure of the Ti6Al4V substrate is shown in Fig. 2a, and it is characterized by beta phase in the matrix of alpha grain structure. The alpha phase is colored lighter by the etchant while the beta phase is colored darker as shown in Fig. 2a. This microstructure is typical of any Ti6Al4V because of the alpha and beta stabilizers contained in the alloy—aluminum and vanadium. This microstructure is what is responsible for the excellent properties of this titanium alloy, and it is responsible for the highest strength-to-weight ratio property possessed by the alloy.

The morphology of the Ti6Al4V powder shown in Fig. 2b is spherical in shape because of the gas atomization process

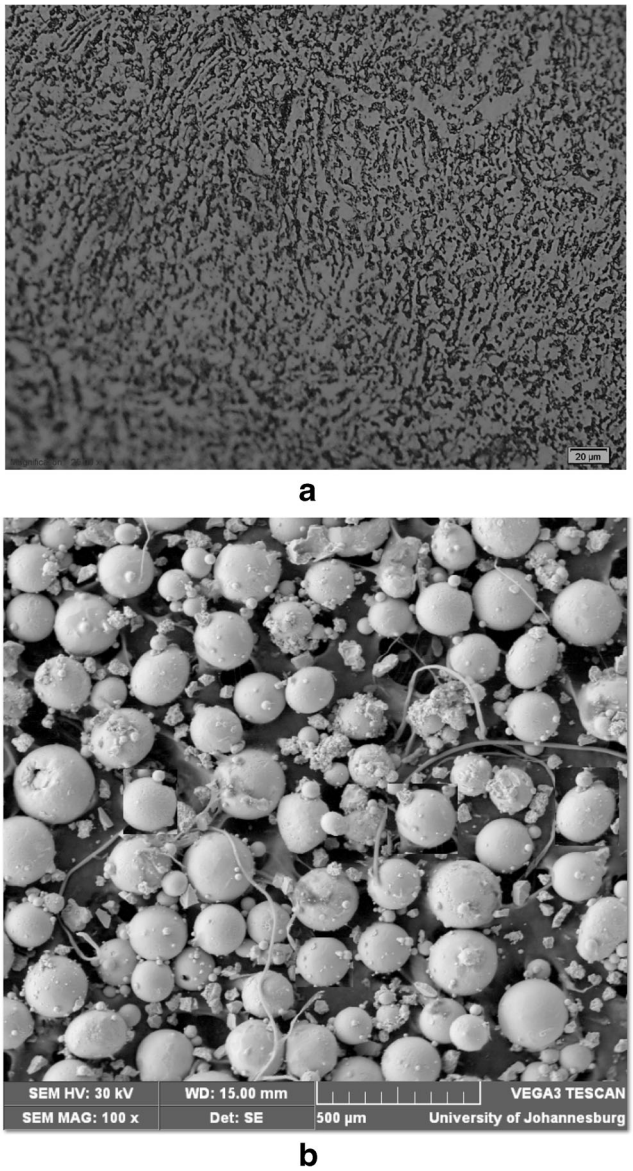

Fig. 2 Micrograph of **a** Ti6Al4V substrate and **b** Ti6Al4V powder

used in producing the powder. Spherical-shaped powders are more favored for additive manufacturing process [28] because it enables proper absorption of the laser energy. The microstructures of the samples produced at scanning speeds of 0.02 and 0.12 m/s and at a powder flow rate of 2.88 g/min are shown in Fig. 3. The microstructure of the sample produced at a scanning speed of 0.02 m/s and powder flow rate of 2.88 g/min consists of thick lath of Widmanstätten (basket woven) alpha grain structure as shown in Fig. 3a and b. The microstructure consists of thick lath of Widmanstätten (basket woven) alpha grain structure. The reason for this type of microstructure is that the cooling rate was very slow. Slow solidification and slow cooling rate are associated with large melt pool that resulted when the scanning speed is low. At low scanning speed, the laser-material interaction time is high which gives more time for the melting of the surface of the

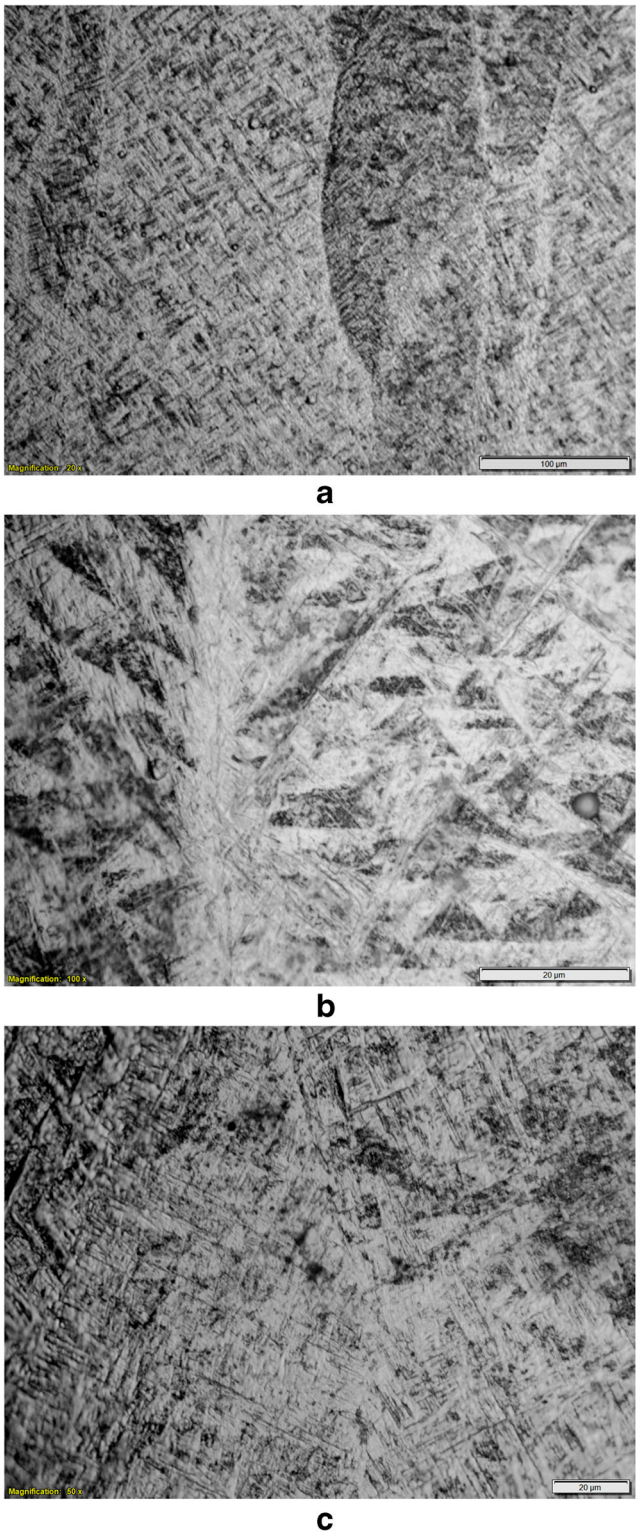

Fig. 3 Micrographs showing the microstructure of samples produced at **a** scanning speed of 0.02 m/s and powder flow rate of 2.88 g/min, **b** (**a**) at higher magnification, **c** scanning speed of 0.12 m/s and powder flow rate of 2.88 g/min

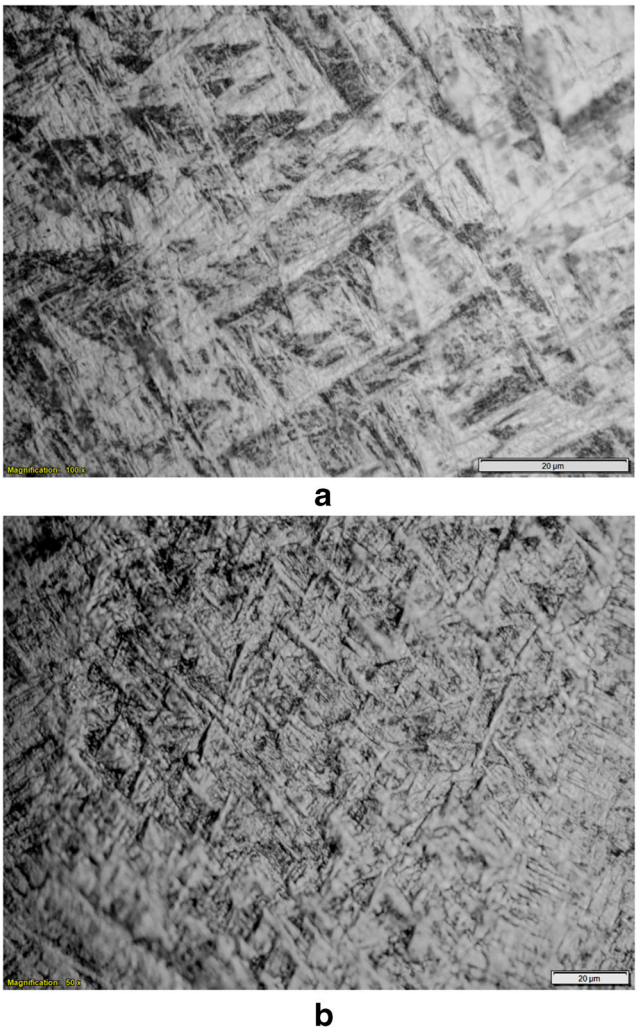

Fig. 4 Micrographs showing the microstructure of samples produced at **a** scanning speed of 0.06 m/s and powder flow rate of 0.72 g/min, **b** scanning speed of 0.06 m/s and powder flow rate of 6.48 g/min

substrate and the deposited powder which resulted in large melt pool. Large melt pool takes longer to solidify and cool down, thereby promoting the formation of Widmanstätten alpha grain structure. A thicker lath of this Widmanstätten alpha is observed at this very low scanning speed which is seen to reduce as the scanning speed was increased. The micrograph shown in Fig. 3b is that of the sample produced at a scanning speed of 0.12 m/s and powder flow rate of 2.88 g/min. The microstructure shows the presence of martensitic grain structure. The martensitic alpha was formed as a result of rapid cooling rate that occurs when the scanning speed is high. At high scanning speed, the laser-material interaction time is small and the melt pool produced at this high scanning speed is also small because there was less time for the laser to melt the surface of the substrate as well as the deposited powder.

This is what caused the solidification and the cooling rate to be faster, which favors the formation of the martensitic alpha grains observed at this high scanning speed.

The effect of the powder flow rate on the microstructure is observed to be similar to those produced with varying

Table 3 Results with varying scanning speeds

Sample label	Scanning speed (m/s)	Powder flow rate (g/min)	Microhardness (HV)	Surface roughness (R_a)
A1	0.02	2.88	330.60	5.5
A2	0.04	2.88	354.05	14.01
A3	0.06	2.88	379.05	18.09
A4	0.08	2.88	405.79	20.93
A5	0.1	2.88	442.02	22.98
A6	0.12	2.88	446.06	23.09

scanning speeds. At low powder flow rate, the delivered powder into the melt pool created by the laser beam on the substrate is low and effective melting took place. The melt pool created is large because the available laser power is large and the delivered powder is small which resulted in more melting of the surface of the substrate. Large melt pool solidifies and cools down slowly which supports the formation of the fine Widmanstätten alpha seen in Fig. 4a. The mixture of Widmanstätten alpha and martensitic alpha grains are seen at high powder flow rate as shown in Fig. 4b. At high powder flow rate, the large available powder for melting does not permit large melting of the substrate materials to occur because the large percentage of the available laser power is consumed by the delivered powder. Which usually results in the creation of moderate melt-pool size? Moderate melt pool causes the solidification and the cooling rate to promote the formation of both the Widmanstätten alpha and martensitic alpha grains to be formed as seen in Fig. 4b. These microstructures are seen to have a direct relationship with the microhardness measured on these samples. The microhardness indentation on the sample at a scanning speed of 0.04 m/s and powder flow rate of 2.88 g/min is shown in Fig. 5.

The graph of microhardness against the scanning speed presented in Fig. 6a shows that the microhardness increased linearly as the scanning speed was increased. This can be correlated to the microstructures that were described above. The low microhardness obtained at low scanning speed is a result of the formation of the Widmanstätten alpha grain structure which is soft. The martensite seen at higher scanning speed is responsible for the higher microhardness obtained at higher scanning speed. The rapid solidification associated with the small melt pool and high scanning speed is responsible for the formation of the martensitic alpha grain structures produced which is hard.

It can be seen from the graph shown in Fig. 6a that the microhardness and the average surface roughness increased as the scanning speed was increased. At low scanning speed, the microhardness was found to be low; this is because of the Widmanstätten alpha grains that are produced at low scanning speed which is characterized by the softness of these grains. As the scanning speed was increased, the microhardness was found to be increased as a result of the presence of the martensitic alpha grains as the scanning speed was increased. Similarly, the average surface roughness was found to increase with the increase in scanning speed as shown in Fig. 6a, although the surface roughness varied non-lineally with the canning speed. At low scanning speed, there was proper melting of the deposited powder due to the high laser-material interaction time and the slow cooling of the melt pool resulted in the low surface roughness values at the low scanning speed. Conversely, at high scanning speed, the rapid cooling could result in the formation of scales on the surface of the deposited sample which could be responsible for the high average surface roughness values observed at high scanning speed.

From Fig. 6b, the microhardness was observed to increase with increase in powder flow rate. The low microhardness seen at the low powder flow rate was a result of the soft Widmanstätten alpha grain structure formed at low powder flow rate due to the large melt pool. The presence of martensitic alpha grain structure, which is hard as seen in the microstructure, in combination with the Widmanstätten alpha grain structure at high powder flow rate could be responsible for the

Table 4 Results with varying powder flow rates

Sample label	Powder flow rate (g/min)	Scanning speed (m/s)	Microhardness (HV)	Surface roughness (R_a)
B1	0. 72	0.06	329.89	3.60
B2	1.44	0.06	346.04	11.04
B3	2.88	0.06	379.05	16.09
B4	4.32	0.06	409.38	19.01
B5	5.76	0.06	438.90	21.76
B6	6.48	0.06	450.59	22.08

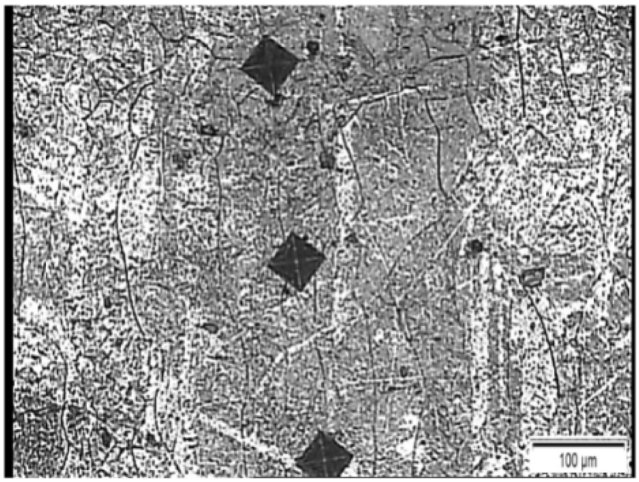

Fig. 5 Micrograph of the sample at a scanning speed of 0.04 m/s and powder flow rate of 2.88 g/min

high microhardness values observed. It could also be a result of the presence of unmelted powder particles in the deposited sample produced at high powder flow rate. If the available laser power is not enough to properly melt the large deposited powder, this could result in higher scanning speed. If this is the case, it is not desirable and there should be a limit to which the powder flow rate should be increased to prevent this from happening. Also, the surface roughness is observed to increase with the increase in powder flow rate as shown in Fig. 6b. At low powder flow rate, the proper melting of the powder and slow solidification as well as slow cooling rate were responsible for the low average surface roughness values obtained. The higher average roughness values seen at high powder flow rate could be a result of the improper melting of the deposited powder at higher powder flow rate, as explained earlier, or it could be a result of scale formation that is associated with rapid cooling of small melt pool. The optimum

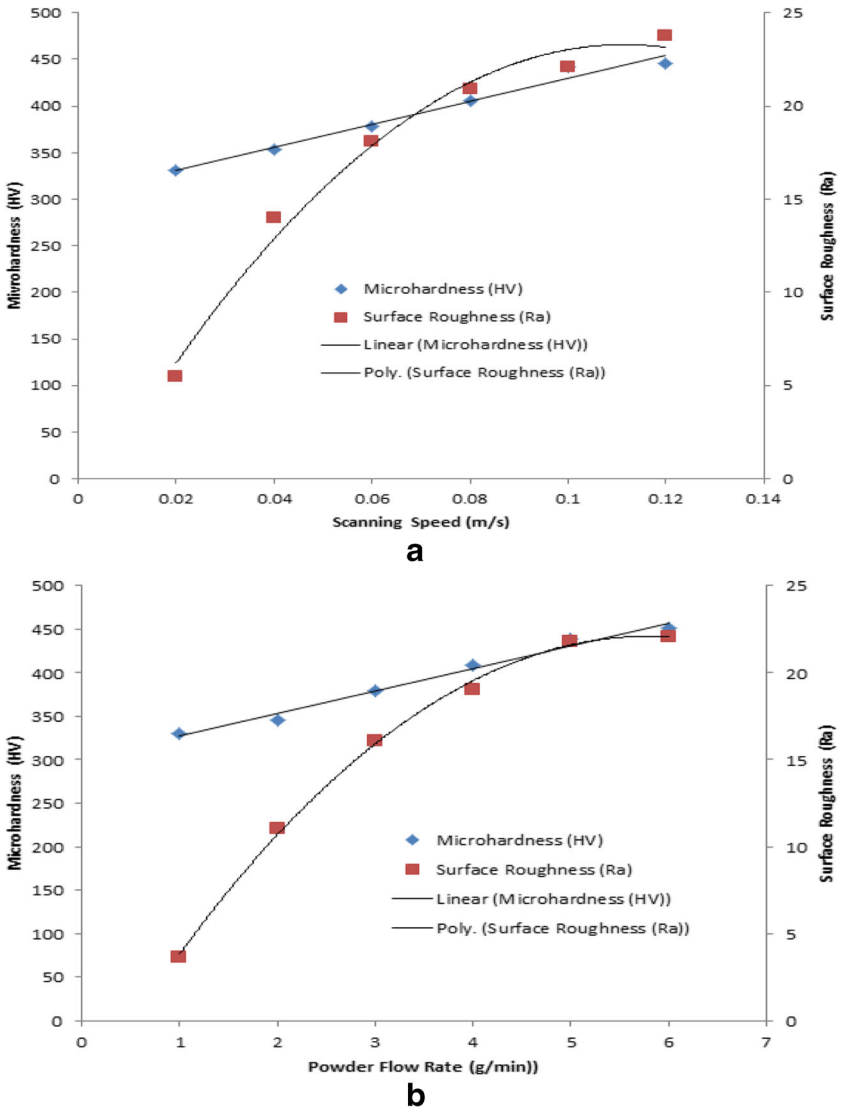

Fig. 6 Graph of microhardness and surface roughness against the **a** scanning speed and **b** powder flow rate

scanning speed and powder flow rate based on the other fixed processing parameters can be seen in Fig. 6a as 0.063 m/s and 2.88 g/min, respectively. The reason for selecting these processing parameters as the optimum processing parameters is that these parameters produce deposit with moderately high microhardness while minimizing the surface roughness value.

5 Conclusion

This study examined the influence of the scanning speed and the powder flow rate on the resulting microstructure, microhardness, and the surface roughness during laser metal deposition process of Ti6Al4V, an important aerospace alloy. By increasing the scanning speed rate, the solidification rate was found to be increased, which in turn results in the formation of microstructures varying from the soft Widmanstätten alpha grain structure to the hard martensitic alpha grain structures. The microhardness and the average surface roughness were found to increase with the increasing scanning speed which was a result of these microstructures. Also, the microhardness and the surface roughness were found to increase as the powder flow rate was increased which could be a result of improper melting of the powder at higher powder flow rate. It can be concluded that the powder flow rate should not be increased too much so as not to result in improper melting of the deposited sample which could be detrimental to the properties of the deposit. The optimum process parameters for the set of parameters considered in this study is the laser power of 3 kW, scanning speed of 0.063 m/s, powder flow rate of 2.88 g/min, and gas flow rate of 2 l/min.

Acknowledgements This work was supported by University of Johannesburg research council and the L'OREAL-UNESCO for Women in Science.

References

1. Scott, J., Gupta, N., Wember, C., Newsom, S., Wohlers, T. and Caffrey, T. (2012*). Additive manufacturing: status and opportunities, Science and Technology Policy Institute*, Available from: https://www.ida.org/stpi/occasionalpapers/papers/AM3D_33012_Final.pdf (Accessed on 11 July 2016)
2. Allen, J. (2006). An investigation into the comparative costs of additive manufacture vs. machine from solid for aero engine parts. In Cost Effective Manufacture via Net-Shape Processing, Meeting Proceedings RTO-MP-AVT-139, Paper 17, pp. 1–10
3. Graf B, Gumenyuk A, Rethmeier M (2012) Laser metal deposition as repair technology for stainless steel and titanium alloys. Phys Procedia 39:376–381
4. Pinkerton AJ, Wang W, Li L (2008) Component repair using laser direct metal deposition. J Eng Manuf 222:827–836
5. Ermachenko AG, Lutfullin RY, Mulyukov RR (2011) Advanced technologies of processing titanium alloys and their applications in industry. RevAdvMater Sci 29:68–82
6. Donachi MJ (2000) Titanium—a technical guide, 2nd edn. ASM International, Metals Park, OH
7. Lütjering G, Williams JC (2003) Titanium. Springer, Berlin
8. Mahamood, R. M., Akinlabi, E. T., Shukla M. and Pityana, S. (2013a). Laser metal deposition of Ti6Al4V: a study on the effect of laser power on microstructure and microhardness. International Multi-conference of Engineering and Computer Science (IMECS 2013), March 2013. 994–999.
9. Bontha, S. (2006). *The effect of process variables on microstructure in laser-deposited materials,* PhD thesis, Mechanical Engineering, Wright State University.
10. Brandl E, Michailov V, Viehweger B, Leyens C (2011) Deposition of Ti–Al–4V using laser and wire, part I: microstructural properties of single beads. Surface & Coatings Technology 206:1120–1129
11. Mahamood RM, Akinlabi ET (2015) Process parameters optimization for material deposition efficiency in laser metal deposited titanium alloy. Lasers in Manufacturing and Materials Processing. doi:10.1007/s40516-015-0020-5
12. Mahamood RM, Akinlabi ET, Shukla M, Pityana S (2014) Characterization of laser deposited Ti6A4V/TiC composite. Lasers in Engineering 29(3–4):197–213
13. Mahamood RM, Akinlabi ET (2015) Effect of laser power and powder flow rate on the wear resistance behaviour of laser metal deposited TiC/Ti6Al4V composites. Materials Today: Proceedings 2(4–5):2679–2686
14. Gao SY, Zhang YZ, Shi LK, Du BL, Xi MZ, Ji HZ (2007) Research on laser direct deposition process of Ti-6Al-4V alloy. Acta Metallurgica Sinica (English Letters) 20:171–180
15. Krantz, D.; Nasla, S.; Byrne, J.; Rosenberger, B. (2001). On-demand spares fabrication during space missions using laser direct metal deposition, USA: AIP.
16. Mahamood RM, Akinlabi ET, Shukla M, Pityana S (2013) Characterizing the effect of laser power density on microstructure, microhardness and surface finish of laser deposited titanium alloy. J Manuf Sci Eng 135(6). doi:10.1115/1.4025737
17. Mahamood RM, Akinlabi ET, Akinlabi SA (2014) Laser power and scanning speed influence on the mechanical property of laser metal deposited titanium-alloy. Lasers in Manufacturing and Materials Processing 2(1):43–55
18. Ng GKL, Jarfors AEW, Bi G, Zheng HY (2009) Porosity formation and gas bubble retention in laser metal deposition. Applied Physics A 97:641–649
19. Pityana, S., Mahamood, R. M., Akinlabi, E. T., and Shukla M. (2013). Gas flow rate and powder flow rate effect on properties of laser metal deposited Ti6Al4V. 2013 International Multi-conference of Engineering and Computer Science (IMECS 2013), March 2013. 848–851.
20. Akinlabi ET, Mahamood RM, Shukla M, Pityana S (2012) Effect of scanning speed on material efficiency of laser metal deposited Ti6Al4V. World Academy of Science and Technology 6:58–62Paris 2012
21. Mahamood RM, Akinlabi ET (2015) Effect of processing parameters on wear resistance property of laser material deposited titanium-alloy composite. Journal of Optoelectronics and Advanced Materials (JOAM) 17(9–10):1348–1360
22. Mahamood, R. M. and Akinlabi, E.T. (2015), Laser metal deposition of functionally graded Ti6Al4V/TiC. Mater Des, 84, 402–410, doi: 10.1016/j.matdes.2015.06.135. (http://www.sciencedirect.com/science/article/pii/S0264127515300265).
23. Mahamood RM, Akinlabi ET (2016) Process parameters optimization for material deposition efficiency in laser metal deposited titanium alloy. Lasers in Manufacturing and Materials Processing 3(1):9–21. doi:10.1007/s40516-015-0020-5

24. Berkmanns, J. and Faerber, M. (2010). *Laser basics, BOC*. Available from: https://boc.com.au/boc_sp/downloads/gas_brochures/BOC_216121_Laser%20Basics_v7.pdf (accessed on 25 July 2016).
25. BS EN ISO 4288:1998, (1998). Geometric product specification (GPS). Surface texture. Profile method: rules and procedures for the assessment of surface texture, BSI
26. E3−11 (2011) Standard guide for preparation of metallographic specimens. ASTM international Book of Standards 03(2011):01. doi:10.1520/E0003-11
27. ASTM E92 - 16. (2016). Standard test method for Vickers hardness and Knoop hardness of metallic materials, ASTM International Book of Standards, 03 (01), doi: 10.1520/E0092-16.
28. Schade, C. T., Murphy T. F. and Walton, C. (2014). Development of atomized powders for additive manufacturing. Powder Metallurgy Word Congress (2014). Accessed on 2nd July 2014 available at: http://www.gkn.com/hoeganaes/media/Tech%20Library/Schade-Atomized%20Powders%20for%20Additive%20Manufacturing%20%281%29.pdf